# WS 2 Nanobuds as a New Hybrid Nanomaterial

**3 AUTHORS:**

Maja Remskar
Jožef Stefan Institute
**61** PUBLICATIONS **1,849** CITATIONS

SEE PROFILE

Marko Virsek
Jožef Stefan Institute
**18** PUBLICATIONS **295** CITATIONS

SEE PROFILE

Adolf Jesih
Jožef Stefan Institute
**60** PUBLICATIONS **1,177** CITATIONS

SEE PROFILE

# WS$_2$ Nanobuds as a New Hybrid Nanomaterial

**Maja Remskar,\* Marko Virsek, and Adolf Jesih**

*Jozef Stefan Institute, Jamova 39, 1000 Ljubljana, Slovenia*

## ABSTRACT

We report on the first inorganic nanobuds: WS$_2$ nanotubes decorated with fullerene-like particles. They were synthesized by sulfurization of W$_5$O$_{14}$ nanowires. The fullerene-like particles nucleate in surface corrugations of the nanowires and grow by a diffusion process simultaneously with the transformation of nanowires into hollow multiwall nanotubes. Electron microscopy data are correlated with details of the transformation process revealing the possible mechanism of the formation of these new complex nanomaterials.

Nanotubes of MoS$_2$ and WS$_2$, first reported in 1992 and 1993 by Tenne's group, were the first inorganic nanotubes, succeeding the discovery of carbon nanotubes (NTs) and launching an intense experimental interest in the field. A variety of nanotubes have been reported, not only consisting of layered compounds possessing a strong sp$^2$ hybridization by analogy with carbon NTs but also of nonlayered materials, like metals and metal oxides.[1−5] In contrast with nanotubes, inorganic fullerene-like (IF) nanoparticles (NPs) are known only in a few families of materials, like WS$_2$,[6] MoS$_2$,[7,8] TaS$_2$,[9] TiS$_2$,[10] BN,[11,12] TiO$_x$,[13] Cs$_2$O,[14] CdCl$_2$,[15] CdI$_2$,[16] and NiBr$_2$.[17] Only in the case of WS$_2$, has production been scaled up to the pilot stage reaching several kg per day. The most efficient methods for producing WS$_2$ nanotubes and IF nanoparticles are via sulfurization of WO$_x$ nanoparticles in a fluidized bed reactor using a stream of H$_2$S gas[18] and template deposition using porous alumina.[19] Other growth techniques make use of electron beam irradiation in a transmission electron microscope,[20] or a scanning tunneling microscope,[21] sono-electrochemical bath reaction,[22] or by and electrochemical deposition from an ethylene glycol solution.[23] Although an important goal is to produce nonagglomerated WS$_2$ fullerene-like materials, the complete transformation of tungsten oxides to hollow nanotubes and fullerenes is an addition technological challenge. The most common phase found encapsulated inside WS$_2$ NPs and nanotubes, after a process of sulfurization to a WS$_2$ structure, is the monoclinic W$_{18}$O$_{49}$ with the largest oxygen deficiency of all the tungsten oxides, the so-called Magneli phases. It is reported that the reduction of the oxide core eventually stops the sulfurization reaction by reducing the oxide to pure tungsten.[24] The remaining tungsten or tungsten oxide in a core of IF NPs contributes

to the shock resistance of the material but makes it less appropriate for use as a lubricant, which is currently the most important application of these nanomaterials. The growth mechanism of IF nanoparticles is proposed to be kinetically controlled by locally limited diffusion inside transition metal oxides or amorphous dichalcogenide NPs, which has led to a conclusion that the fullerene-like geometry can be obtained only inside a confined geometry, in a so-called "outside in" growth mode.

We present here evidence that the spherical geometry of WS$_2$ is an intrinsic property and can be obtained also by rate-limited diffusion from a bulk reservoir of materials. The porous structure of the W$_5$O$_{14}$ precursor crystals enables a complete transformation into WS$_2$ nanotubes, whereas longitudinal surface corrugations create line diffusion paths for tungsten atoms feeding the growth of WS$_2$ nanobuds on the surface of the nanotubes.

Nanowires of W$_5$O$_{14}$ have been synthesized by a chemical transport technique using nickel as a growth promoter.[25] Light-blue crystals with metallic conductivity and a specific resistivity of 27 $\mu\Omega$ cm grow typically to several millimeters in length and up to 200 nm in diameter. This rarely synthesized phase, which was first reported as a homogeneous phase in 1978 by McColm et al.,[26] although in the meantime has only been found in traces, is here prepared as a highly homogeneous material (Figure 1). The presence of nickel was found to be crucial in the formation of W$_5$O$_{14}$ nanowires, because the Ni(OH)$_2$ phase situated at the interface between WS$_2$ plate-like base and the sub-oxide needles, enables fast tungsten diffusion, which leads to highly anisotropic growth. The well ordered nanoporous structure contains hexagonal and pentagonal tunnels (Figure 1c), which can serve as diffusion paths for foreign intercalated species or self-intercalated tungsten. The unit cell was determined to be tetragonal with parameters: $a = 2.333 \pm 0.001$ nm, $c$

\* Corresponding author. Address: Solid State Physics Department, Jozef Stefan Institute, Jamova 39, SI- 1000 Ljubljana, Slovenia. Tel.: 386 1 4773 921. Fax: 386 1 4773 191. E-mail: maja.remskar@ijs.si.
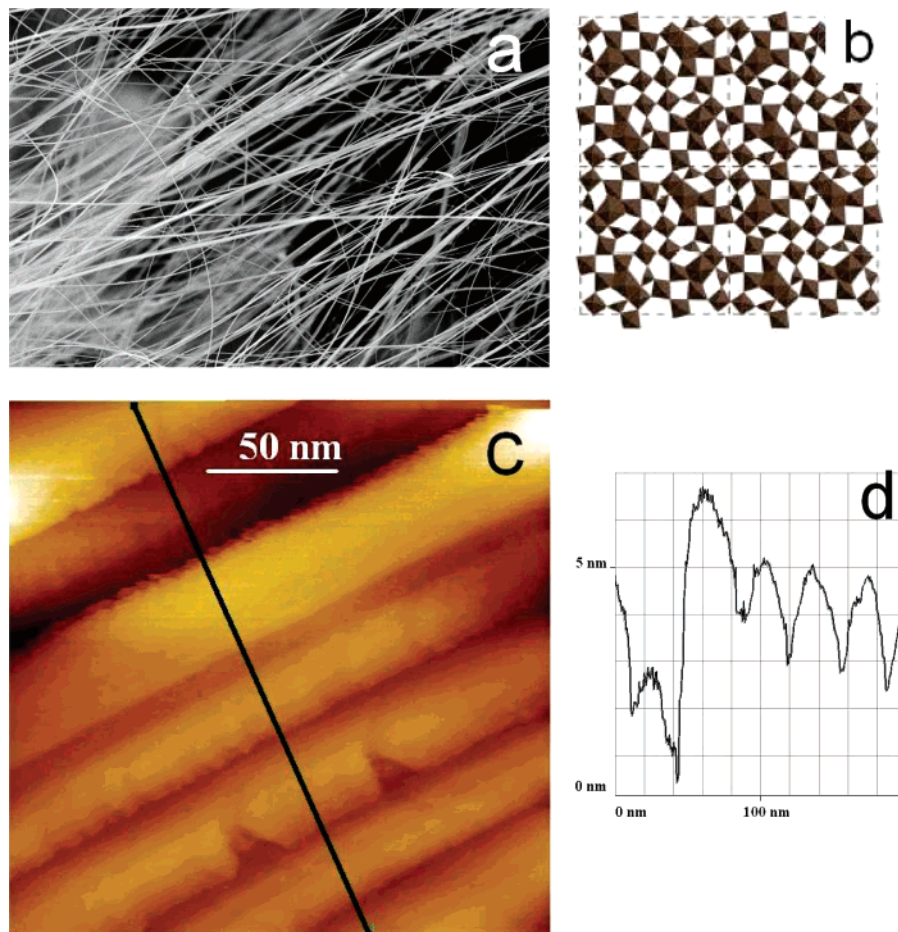
**Figure 1.** (a) Nanowires of $W_5O_{14}$ with diameter up to 100 nm grown as rigid fibers up to a few mm in length. (b) Schematically presented cross-section of a nanowire with pentagonal and hexagonal tunnels along the longitudinal axis.[27] (c) STM image ($U_T = 0.5$ V; $I_T = 0.5$ nA) of surface corrugations oriented along the needle axis with the corresponding line profile (d).

$= 0.3797 \pm 0.0001$ nm and $P42_1m$ space group. The phase is isostructural with $Mo_5O_{14}$, although without the superlattice cell typical for $Mo_5O_{14}$. Scanning tunneling microscopy (STM) revealed surface corrugations of the needles oriented in parallel with the needle axis (Figure 1c). The folds are a few nanometers in depth and quiet homogeneous in width along the nanowire longitudinal direction.

Nanowires of $W_5O_{14}$ in milligram quantities are sulfurized in a mixture of 1% $H_2$, 1% $H_2S$, and 98% Ar gases with a flow rate of 30 mL/min at 1050 K for 2 h. Thereafter the material is removed from the hot zone and cooled to room-temperature still under the flow of gases. The transformed nanofibres, which then have a metallic luster, are character-ized by field emission transmisson electron microscopy (200 keV Jeol 2010 F), ultrahigh vacuum scanning tunneling and atomic force microscopy (UHV-AFM/STM, Omicron), X-ray diffraction (Siemens D-5000), and field emission scanning electron microscopy (FE-SEM, Supra 35 VP, Carl Zeiss). The material is composed mostly of $WS_2$ and some traces of $NiS_x$. The $WS_2$ nanotubes are typically decorated with $WS_2$ fullerene-like particles (Figure 2a), but it is possible to find some nondecorated nanotubes too (Figure 2b). Several nanotubes grow from one precursor nanowire, which enables insight into the transformation process. The reaction leads to a complete longitudinal split of the precursor crystal with simultaneous covering of the newly exposed surface with $WS_2$ layers, which limits the diffusion to the separated section. Diffusion along the surface corrugations repairs the eventual inhomogeneity of the splitting process and makes the growth of long nanotubes with nearly equal wall thickness possible (Figure 2b). In some cases, the tube bundles can even cross (Figure 2c), which would not be possible without a strong redistribution of material. If the diffusion is locally terminated, these tubes are strongly deformed and the splitting process does not fully complete. (Figure 2d). The ability that the precursors do not completely control the minimal size of the final product, as it usually happens in the template growth, is important due to technological issues to produce nanotubes as narrow as possible.

The fullerene-like particles always grow attached to the surface of needles but in a random way regarding their appearance and spacing. Several morphologies have been identified simultaneously, apparently similar to the buds in plants. In the early stage, the thin-walled buds become round on one side and narrow at the contact area, growing elongated in the direction of the supporting nanotube (Figure 3a). These formations reveal that the material needed for growth is provided by diffusion, which is most likely along the surface and bulk channels of the precursor crystals. The next stage is growth of faceted nanoparticles (Figure 3b) with thicker
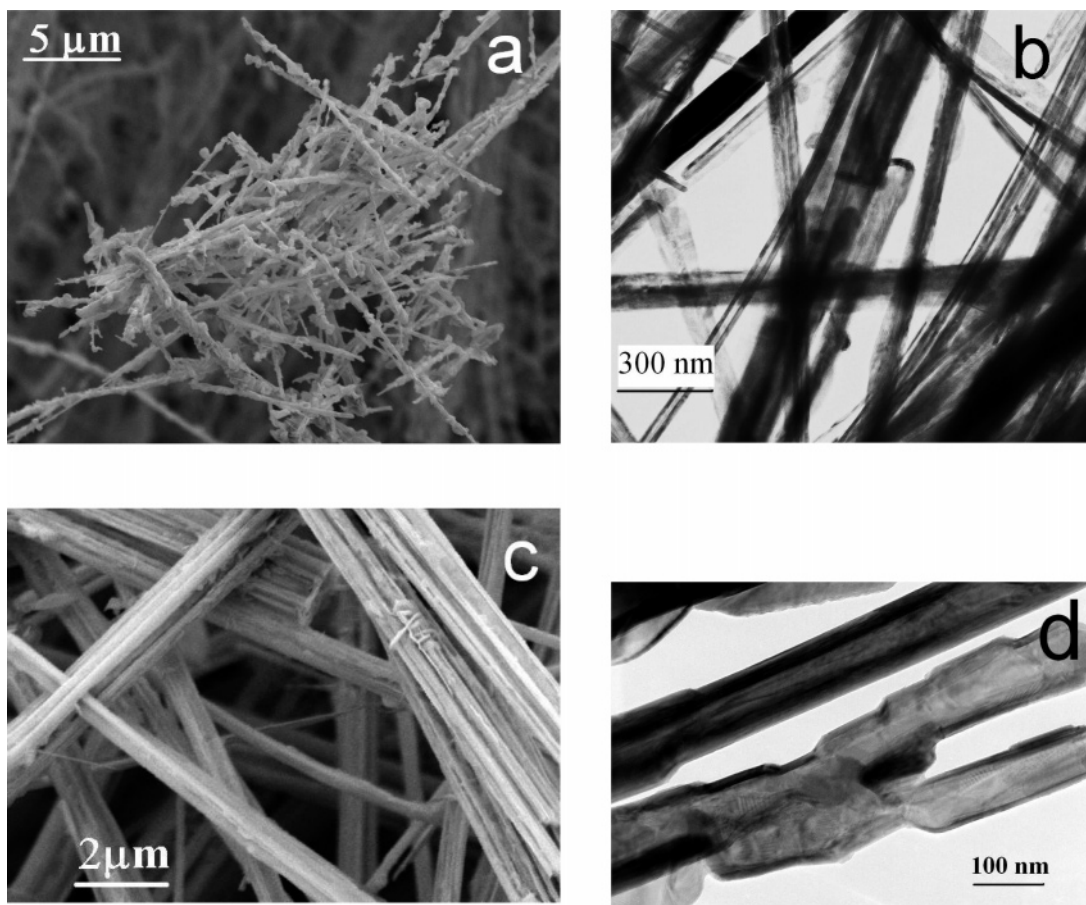
**Figure 2.** (a) SEM image of $WS_2$ nanotubes decorated with $WS_2$ fullerene-like particles. (b) TEM image of bundles of dome-capped nanotubes with diameter bellow 50 nm. (c) SEM image of two crossed bundles of nanotubes and (d) splitting area of a precursor crystal into two parallel nanotubes.

walls, which are still narrowed at the contact area, so that further diffusion is still possible. In some cases, a kind of secondary nucleation has been observed, i.e., some fullerenes grow on the surface of twinned fullerenes, where the diffusion paths are developing at the interface folds. In this stage, the walls are thicker and the particles are more spherically shaped into the nearly ball-like morphology (Figure 3c). The fullerene-like particles can grow up to several hundreds of nanometers, which exceeds the dimensions of those produced by template techniques from $WO_x$ nanoparticles.

The nanotubes grow in the relaxed 2Hb stacking, which contains two S−W−S molecular layers in the unit cell (Figure 3a-inset). The unit cell was found not to be only a crystallographic term but conditions also the stability during the process of growth. We found that the walls of the nanotubes frequently consist of an even number of molecular layers. For example, the wall thickness of a nanotube presented at Figure 3a, shrinks from eight to four molecular layers in steps by two molecular layers. The other example originates from the sulfurization process per se. Figure 3b shows the first stage of transformation. The dark rectangular crystal is the original $W_5O_{14}$ crystal with the first two S−W−S layers enveloping it. The substrate is a thin flake of $WS_2$. The separation of the envelope from the oxide single crystal is present only at one edge and is evidence that the nanotube walls grow from the inside (at the right side of the

envelope) by two molecular layers simultaneously. The double-layer-by-double-layer growth mode was reported in Au-alloyed $WS_2$ nanotubes and confirms the stabilization of a hexagonal 2Hb polytypic stacking.[28]

The role of conductivity in the sulfurization process is not well established, but it is known that, in large scale production in a fluidized bed reactor,[6,7] $WO_3$ is reduced first. This is usually obtained using $H_2$ in the mixture of the sulfurization gases. As the sulfurization process continues, the material composition advances through the homologous series with the formula $W_nO_{3n-1}$ until the most reduced $W_{18}O_{49}$ phase is reached and slowly transforms to hollow $WS_2$ nanoparticles. $W_5O_{14}$ has been found in traces in the resulting oxide cores,[27] but it has not been utilized as a starting material until now. Most of the substoichiometric tungsten oxides show improved electronic conductivity with respect to nonconductive $WO_3$, which has a resistance on the order of $1 \times 10^5$ Ω cm.[29] As an example, $W_{18}O_{48}$ is 8 orders of magnitude more conductive, $1.75 \times 10^{-3}$ Ω cm,[30] whereas $W_5O_{14}$ is 10 times more conductive, $27 \times 10^{-6}$ Ω cm.[26] Creation of substoichiometric oxides is coupled with the creation of charged oxygen vacancies; therefore, it is very important that the oxides are neutralized by a good electrical ground. In the process of sulfurization, the tungsten oxidation number has to change from $6^+$ in stoichiometric $WO_3$ to $4^+$ in $WS_2$ or, in our particular case, from the average value of
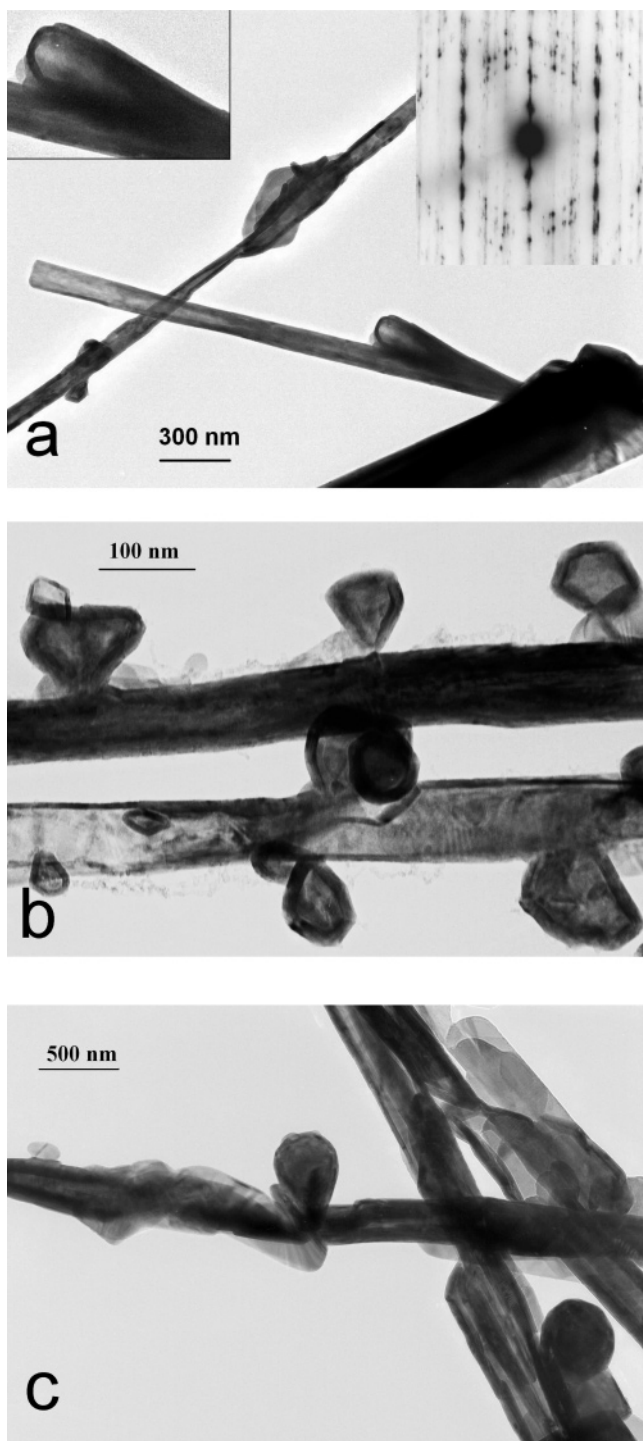
**Figure 3.** WS$_2$ nanobuds: (a) an early stage of growth with typically elongated thin walled buds along the nanotube support, which serves as a reservoir of material. The nanotube grow in the relaxed hexagonal 2Hb stacking (inset). (b) Some faceted nanoparticles joined to the supported thin-walled nanotube with their V-shaped parts. (c) The final stage of growth with nearly spherical thick-walled fullerenes.

5.6$^+$ in W$_5$O$_{14}$[25] to 4$^+$ in WS$_2$. It is obvious that a redistribution of charge carriers is needed for the complete transformation process, so an easy electron transport along the precursor crystals enables an efficient transformation.

Scanning tunneling microscopy of W$_5$O$_{14}$ nanowires reveals a strong surface corrugation with a period 3−8 times
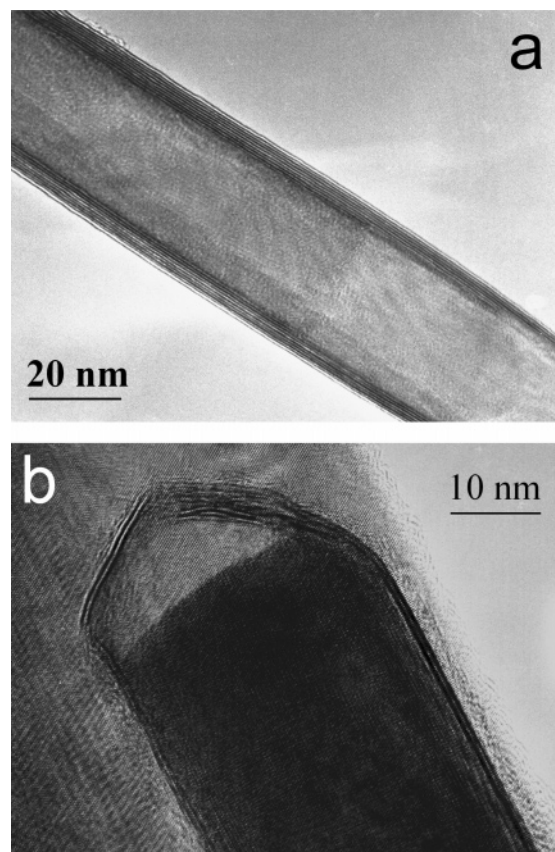


**Figure 4.** (a) WS$_2$ nanotubes with 8, 6, and 4 molecular layers in wall thickness. (b) The first step of sulfurization with a two-molecular-layers-thick WS$_2$ envelope around a W$_5$O$_{14}$ precursor crystal. The envelope wall grows thick from the inside.

larger than the corrugation found on the surface of W$_{18}$O$_{49}$ nanowires. An accurate depth of the corrugation is difficult to measure because of the uncertain curvature of the STM tip; however, corrugations with smaller periods appear to be shallower. The vapor pressure of the volatile WO$_{3-x}$·$n$H$_2$O hydrate (H$_2$O is a side product of the sulfurization process) in nanofolds (surfaces with negative curvature) is lowered with respect to sites with positive curvature according to the Kelvin equation.[31] Nevertheless, it is possible to predict that the hydrate vapor stagnates in the channels relative to sites which have positive curvature. Positive curvature sites are exposed to currents of gas flow and therefore promote the release of the hydrate molecules during the sulfurization process until the moment when the surface is protected with the first two WS$_2$ layers. The presence of the hydrate vapor in the folds influences the local partial pressures of the reactive gases and might circumvent the complete growth of the protective WS$_2$ layers in the folds. The channels deepen until the moment when preferential "etching" of the precursor crystals along the folds completes and the original nanowire splits apart. The tunnel structure of the precursor W$_5$O$_{14}$ crystals makes the progress easy. Further, the WO$_{3-x}$·$n$H$_2$O clusters in the folds and in the presence of a reactive and turbulent H$_2$/H$_2$S−Ar mixture enable a nucleation of fullerene-like particles therein, likely triggered by local defects, where a condensation of WS$_2$ starts. The slope of a channel explains the V-shape of the fullerenes in the

early stages of growth. The diffusion process, confined within narrowing and deepening channels provides the $WS_2$ particles with tungsten during the growth, most likely through the straits which connect them to the central nanowire, which is then slowly transformed to the hollow $WS_2$ nanotube. The existence of thin-walled nanotubes with a large lack of material with respect to the precursor nanowires supports the conclusion that the nanobuds grow on account of the supported nanotubes, implying their growth is thermodynamically preferential under these conditions. Spontaneous growth of curved and self-terminated layers suggests that such a geometry forms as a results of an intrinsic property of the compound at the nanoscale.

In summary, $W_5O_{14}$ nanowires with a typical tunnel structure were used as precursor crystals for growth of long, thin-walled $WS_2$ nanotubes. These nanotubes are decorated with $WS_2$ fullerene-like particles forming the first inorganic "nanobuds", named in analogy with recently published carbon nanobuds.[32] These $WS_2$ fullerenes grow by a diffusion process along surface corrugations and by assistance of a tunnel structure within the nanowires. The growth mechanism for the formation of nanobuds from elongated forms into faceted then final spherical shapes is explained by nucleation and growth of fullerenes seeded within the surface folds. Due to a selective reaction along the surface channels which promotes longitudinal cleavage of the precursors, several nanotubes can grow from a single nanowire. The nanowires were found to be completely transformed to hollow nanoparticles and nanotubes. Good metallic conductance of the $W_5O_{14}$ nanowires is obviously important for the completion of the sulfurization process. The transformation starts with simultaneous growth of two $WS_2$ molecular layers. This observation and some examples of tubes with walls composed of even numbers of molecular layers support the diffraction patterns, which reveal that the hexagonal 2Hb structure with two $WS_2$ layers in the unit cell is a thermodynamically stable polytype under these conditions. There are some indications that the growth of nanobuds on account of the supported nanotubes is thermodynamically preferential. Relatively simple synthesis can be upgraded for bulk production of $WS_2$ nanobuds, which represent a new type of complex nanomaterial with possible applications as lubricants, as catalyst, in polymer composites, as electron field emitters, etc.

## References

(1) Tenne, R. *Nat. Nanotechnol.* **2006**, *1*, 103.
(2) Remskar, M. *Adv. Mater.* **2004**, *16*, 1497.
(3) Enyashin, A. N.; Gemming, S.; Seifert, G. *Eur. Phys. J.*, *Special Topics* **2007**, *149*, 103−125.
(4) Cheng, F.; Chen, J. *J. Mater. Res.* **2006**, *21*, 2744.
(5) Rao, C. N. R.; Nath, M. *Dalton Trans.* **2003**, *1*, 1.
(6) Tenne, R.; Margulis, L.; Genut, M.; Hodes, G. *Nature* **1992**, *360*, 444.
(7) Margulis, L.; Salitra, G.; Tenne, R.; Talianker, M. *Nature* **1993**, *365*, 113.
(8) Feldman, Y.; Wasserman, E.; Srolovitz, D. J.; Tenne, R. *Science* **1995**, *267*, 222.
(9) Schuffenhauer, C.; Parkinson, B. A.; Jin-Phillipp, N. Y.; Joly-Pottuz, L.; Martin, J. M.; Popovitz-Biro, R.; Tenne, R. *Small* **2005**, *1*, 1100.
(10) Margolin, A.; Popovitz-Biro, R.; Albu-Yaron, A.; Moshkovich, A.; Rapoport, L.; Tenne, R. *Curr. Nanosci.* **2005**, *1*, 253.
(11) Jensen, F.; Toftlund, H. *Chem. Phys. Lett.* **1993**, *201*, 95.
(12) Stéphan, O.; Bando, Y.; Loiseau, A.; Willaime, F.; Shramchenko, N.; Tamiya, T.; Sato, T. *Appl. Phys. A* **1998**, *67*, 107.
(13) Ducati, C.; Barborini, E.; Vinati, S.; Milani, P.; Midgley, P. A. *Appl. Phys. Lett.* **2005**, *87*, 201906.
(14) Albu-Yaron, A.; Arad, T.; Popovitz-Biro, R.; Bar-Sadan, M.; Prior, Y.; Jansen, M.; Tenne, R. *Angew. Chem. Intl. Ed.* **2005**, *44*, 4169.
(15) Popovitz-Biro, R.; Twersky, A.; Rosenfeld Hacohen, Y.; Tenne, R. *Isr. J. Chem.* **2001**, *41*, 7.
(16) Popovitz-Biro, R.; Sallacan, N.; Tenne, R. *J. Mater. Chem.* **2003**, *13*, 1631.
(17) Bar-Sadan, M.; Popovitz-Biro, R.; Prior, Y.; Tenne, R. *Mater. Res. Bull.* **2006**, *41*, 2137.
(18) Rothschild, A.; Sloan, J.; Tenne, R. *J. Am. Chem. Soc.* **2000**, *122*, 5169.
(19) Nath, M.; Govindaray, A.; Rao, C. N. R. *Adv. Mater.* **2001**, *13*, 283.
(20) Jose-Yacaman, M.; Lopez, H.; Santiago, P.; Galvan, D. H.; Garzon, I. L.; Reyes, A. *Appl. Phys. Lett.* **1996**, *69*, 1065.
(21) Homyonfer, M.; Mastai, Y.; Hershfinkel, M.; Volterra, V.; Hutchison, J. L.; Tenne, R. *J. Am. Chem. Soc.* **1996**, *118*, 7804.
(22) Mastai, Y.; Homyonfer, M.; Gedanken, A.; Hodes, G. *Adv. Mater.* **1999**, *11*, 1010.
(23) Albu-Yaron, A.; Levy-Clement, C.; Hutchison, J. L. *Electrochem. Solid-State Lett.* **1999**, *2*, 627.
(24) Krivovichev, S. V.; Kahlenberg, V.; Kaindl, R.; Mersdorf, E.; Tananaev, I. G.; Myasoedov, B. F. *Angew. Chem., Int. Ed.* **2005**, *44*, 1134.
(25) Remskar, M.; Kovač, J.; Viršek, M.; Mrak, M.; Jesih, A.; Seabaugh, A. *Adv. Funct. Mater.* **2007**, *17*, 1974.
(26) McColm, I. J.; Steadman, R.; Wilson, S. J. *J.Solid State Chem.* **1978**, *23*, 33.
(27) Frey, G. L.; Rothschild, A.; Sloan, J.; Rosentsveig, R.; Popovitz-Biro, R.; Tenne, R. *J. Solid-State Chem.* **2001**, *162*, 300.
(28) Remskar, M.; Skraba, Z.; Stadelmann, P.; Levy, F. *Adv. Mater.* **2000**, *12*, 814.
(29) Viswanathan, K.; Brandt, K.; Salje, E. *J. Solid State Chem.* **1981**, *36*, 45.
(30) Miyakawa, M.; Kawamura, K. I.; Hosono, H.; Kawazoe, H. *J. Appl. Phys.* **1998**, *84*, 5610.
(31) Kelvin equation: $\ln(p/p_0) = -(2\gamma V_m/rRT)$, where $p$ is the actual vapor pressure, $p_0$ is the saturated vapour pressure, $\gamma$ is the surface tension, $V_m$ is the molar volume, $R$ is the universal gas constant, $r$ is the radius of the channel, and $T$ is the absolute temperature.
(32) Nasibulin, A. G.; et al. *Nat. Nanotechnol.* **2007**, *2*, 156.

NL0719426